

Beamlet-free treatment planning

Beamlet-free optimization for Monte Carlo based treatment planning in proton therapy

Danah Pross,¹ Sophie Wuyckens,¹ Sylvain Deffet,¹ Edmond Sterpin,^{1,2,3} John A. Lee,¹ and Kevin Souris^{1,4}

¹*Université catholique de Louvain, Institut de Recherche Expérimentale et Clinique (IREC), Center of Molecular Imaging, Radiotherapy and Oncology, Louvain-La-Neuve, 1348, Belgium*

²*KU Leuven, Department of Oncology, Laboratory of Experimental Radiotherapy, Leuven, 3000, Belgium*

³*Particle Therapy Interuniversity Center Leuven - PARTICLE, Leuven, 3000, Belgium*

⁴*Ion Beam Applications SA, Louvain-La-Neuve, 1348, Belgium*

(Dated: 18 April 2023)

Background: Dose calculation and optimization algorithms in proton therapy treatment planning often have high computational requirements regarding time and memory. This can hinder the implementation of efficient workflows in clinics and prevent the use of new, elaborate treatment techniques aiming to improve clinical outcomes like robust optimization, arc and adaptive proton therapy.

Purpose: A new method, namely, the beamlet-free algorithm, is presented to address the aforementioned issue by combining Monte Carlo dose calculation and optimization into a single algorithm and omitting the calculation of the time-consuming and costly dose influence matrix.

Methods: The beamlet-free algorithm simulates the dose in proton batches of randomly chosen spots and evaluates their relative impact on the objective function at each iteration. Based on the approximated gradient, the spot weights are then updated and used to generate a new spot probability distribution. The beamlet-free method is compared against a conventional, beamlet-based treatment planning algorithm on a brain case.

Results: The beamlet-free algorithm maintained a comparable plan quality while reducing the computation time by 70% and the peak memory usage by 95%.

Conclusion: The implementation of a beamlet-free treatment planning algorithm for proton therapy is feasible and capable of achieving a considerable reduction of time and memory requirements.

Keywords: Proton therapy, optimization, treatment planning, beamlet-free, stochastic gradient descent, micro-optimization

I. INTRODUCTION

In proton therapy, the state-of-the-art is to treat patients with intensity modulated proton therapy¹ (IMPT) using pencil beam scanning. Treatment planning typically involves the precalculation of individual beamlet dose distributions and subsequent optimization of their respective intensity. The total dose to voxel i is then given as the linear combination of these elementary dose distributions

$$d_i = \sum_j D_{ij}x_j \quad (1)$$

with D_{ij} as the individual beamlet dose contribution of spot j to voxel i and x_j its corresponding intensity ('spot weight'). The dose influence matrix D is the concatenation of the beamlet dose distributions and usually reaches considerable size, due to the large number of spots in IMPT.

While dose calculations can be performed using fast analytical dose calculation algorithms², their accuracy falls short of the more elaborate Monte Carlo methods^{3,4}. The drawback of MC dose engines is their high demand of computational resources that, especially for large numbers of spots, can prolong treatment planning time considerably. It is therefore an ongoing effort to reduce computation time for MC methods and several fast MC dose engines have been introduced, often based on CPU (Central Processing Unit) or GPU (Graphical Processing Unit) parallelization⁵⁻¹⁰.

The storage of the beamlet dose distributions in the dose influence matrix, necessary for optimization, also puts considerable strain on the computers memory capacities¹¹.

Besides the time expended on the repeated calls to the dose calculation engine, the optimization algorithm also places high demands on the computational resources and prolongs computation time, due to the very costly multiplications with the large dose influence matrix involved in the gradient computation.

These high computational demands, both with respect to computation time and memory usage, are hindrances in clinical routines that require to be addressed to enable efficient workflows when a MC dose engine is involved. These problems become additionally exacerbated in study cases that require a large number of beamlets, such as robust optimization, adaptive proton therapy or arc proton therapy. These increasingly elaborate methods seek

to improve treatment quality by reducing dose to organs at risk (OAR) and ensuring target coverage, but are limited by the current computational demands.

The aim of this work is to present a new method of treatment plan optimization that substantially reduces the required computation time and memory, while maintaining the plan quality. The approach combines MC dose calculation and spot weight optimization into a single efficient algorithm. This algorithm is referred to as beamlet-free algorithm since it does not require the computation of individual beamlet dose distributions. The method is applied here to proton therapy with pencil beam scanning, where the number of beamlets is typically higher than in photon therapy and where the superior accuracy of MC methods over analytical dose calculation algorithms is especially beneficial due to the steep dose gradients involved.

II. METHODS

II.A. Cost function

Following a classical approach, the objectives penalize deviations of the dose from a reference value in a region of interest (ROI)¹². For example, to enforce a prescribed minimum dose b_{\min} , the following objective term may be minimized:

$$f_{\min}(\mathbf{d}) = \frac{1}{N_r} \sum_{i=1}^{N_r} \min(0, d_i(\mathbf{x}) - b_{\min})^2, \quad (2)$$

where $N_r = |ROI|$ is the number of voxel in the ROI. A similar objective may be used to enforce a maximum dose b_{\max} :

$$f_{\max}(\mathbf{d}) = \frac{1}{N_r} \sum_{i=1}^{N_r} \max(0, d_i(\mathbf{x}) - b_{\max})^2. \quad (3)$$

Beamlet-free treatment planning

Several objectives may be defined. Hence, the general treatment plan optimization problem takes the following form:

$$\min \quad F(\mathbf{x}) = \sum_k f_k(\mathbf{d}) \quad (4)$$

$$\text{s.t. } \mathbf{x} \geq 0 \text{ ,} \quad (5)$$

where the index k iterates over the objectives and $f_k(\mathbf{d})$ are either $f_{\min}(\mathbf{d})$ or $f_{\max}(\mathbf{d})$ depending on the objective type.

II.B. Beamlet-free algorithm

The idea of beamlet-free optimization is based on continually and incrementally evaluating the objective function while the dose is being simulated. Instead of computing each individual beamlet dose distribution, the dose is continually scored during the MC simulation of the proton batches and directly added to a total dose distribution. Consequently, spot weights in their original sense as modulation factors cannot exist anymore. The equivalent of the original spot weights with respect to the final dose output would be the number of protons simulated towards each spot. To optimize this quantity during the ongoing dose simulation, a set of unnormalized probabilities p is introduced, that are used to generate a spot probability distribution P .

In each iteration of the proposed algorithm, a spot is randomly sampled from this probability distribution P . A batch of protons is simulated towards the chosen spot and the impact on the objective function is calculated to estimate the gradient of the objective function with respect to the probability of the chosen spot.

After all protons of the batch have been simulated, the estimated gradient, with respect to the sampled spot, is used to update the spot probability, similarly to Stochastic Gradient Descent (SGD)¹³.

This yields Algorithm 1, where p_j is the probability for a spot j , P is the corresponding

probability distribution, h is a step size, c is the batch cost calculated as

$$c = \sum_i \sum_k F(d_{i,k-1}) - F(d_{i,k}) \quad (6)$$

with i an index iterating over all voxel, k an index over all proton contributions in a batch, $F(\cdot)$ the objective function as described in equation 4 and $d_{i,k-1}$ and $d_{i,k}$ as the normalized dose to voxel i prior to and after the contribution of particle k . The particle cost calculated in 6 corresponds to the finite difference approximation of the objective function gradient.

The normalization of the dose during the cost computation is necessary to evaluate the relative impact of simulating particles to a given spot j . The total, unnormalized dose is multiplied with a normalization coefficient $n(\mathbf{d}) = \frac{\hat{d}}{b}$ where \hat{d} is the mean target dose and b is the prescribed target dose.

Algorithm 1 Beamlet-free algorithm

- 1: Initialize spot probability vector \mathbf{p} to unit values
 - 2: Generate probability distribution $P(\mathbf{p})$
 - 3: Set $n_{\text{simulated}} \leftarrow 0$
 - 4: **while** $n_{\text{simulated}} \leq n_{\text{total}}$ **do**
 - 5: Sample spot j from P
 - 6: Initiate a batch of n_{batch} particles for spot j
 - 7: Initialize cost $c \leftarrow 0$
 - 8: **for** $k \leq n_{\text{batch}}$ **do**
 - 9: Simulate particle k
 - 10: Update cost $c \leftarrow c + \sum_{i,k} F(d_{i,k-1}) - F(d_{i,k})$
 - 11: $n_{\text{simulated}} \leftarrow n_{\text{simulated}} + 1$
 - 12: **end for**
 - 13: Update spot probability: $p_j \leftarrow p_j - hc$
 - 14: **end while**
-

The quantity to be optimized in this procedure is the spot probability \mathbf{p} , which is stochastically linked to the number of protons simulated toward the corresponding spots, the spot weight \mathbf{x} . The objective function is evaluated over the total dose distribution \mathbf{d} , which depends on \mathbf{x} , and only indirectly on \mathbf{p} . The finite difference approximation in 6 concerns the gradient of the objective function with respect to \mathbf{x} .

There are therefore two separate stochastic processes taking place, the MC simulation generating the dose distribution and the spot sampling at the beginning of each iteration which

causes the distribution of protons per spot, \mathbf{x} , and the probability distribution P to converge towards the same final distribution.

The beamlet-free algorithm was implemented in C around the existing, fast Monte Carlo code MCsquare⁹.

II.C. Phantom data

The beamlet-free method is expected to improve both computation time and memory usage when large numbers of beamlets are involved. To highlight its benefits and limitations, a complexity analysis was performed. Simulations are performed on a water phantom containing a target region of various sizes. The phantom is represented in figure 1. The multiple target sizes result in geometries with varying numbers of spots. Spot and layer spacing are set to 4 mm and a target margin of 6 mm is applied. The influence of the number of spots on computation time and memory usage are investigated.

A single beam with couch and gantry angles of 0° is used for the analysis. The water phantom has dimensions of $150 \times 150 \times 150$ mm³ and the target region is cubic, with the center located at a depth of 110 mm in beam direction and side lengths ranging between 20 mm and 60 mm. A representation of the water phantom can be found in figure 1.

Simulations are repeated 5 times to estimate the impact of statistical fluctuations.

II.D. Patient data

To demonstrate the high potential of the beamlet-free algorithm, we chose to benchmark it against a conventional, beamlet-based gradient descent optimization algorithm. A brain case (base-of-skull tumor) was chosen for the comparison. Local ethics committee approval was obtained for the use of the patient data. A treatment plan was generated using a three-beam combination at a fixed gantry angle $G = 90^\circ$ and rotating the couch angle C at 0° , 270° and 315° . A total of 9812 spots compose the plan. The ROIs upon which optimization objectives are placed are the clinical target volume (CTV), optical chiasm (OC), brain stem (BS), right optical nerve (RON) and left optical nerve (LON). The optimization objectives are listed in

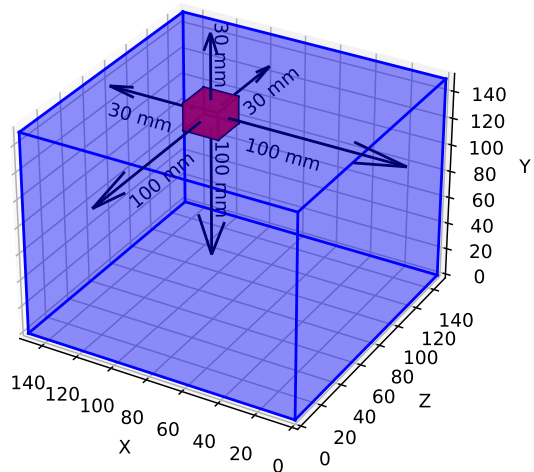


FIG. 1: Water phantom used for the scaling analysis. An exemplary target region with side length of 20 mm is represented in red.

table I.

The treatment plan optimization is performed using the in-house developed, research treat-

TABLE I: Optimization objectives

ROI	Objective Type	Dose limit	Weight
PTV	D_{\min}	54.0	5
PTV	D_{\max}	54.0	5
OC	D_{\max}	60.0	1
BS	D_{\max}	55.0	1
RON	D_{\max}	55.0	1
LON	D_{\max}	55.0	1

ment planning system OpenTPS¹⁴ which can incorporate both the beamlet-free method as well as established optimization algorithms such as second order methods like the BFGS algorithm^{15–18}.

II.E. Optimization parameters

The total number of particles needed in the Monte Carlo simulation, depend on the number of spots. For the water phantom, a number of 40 million primary protons was chosen, which

Beamlet-free treatment planning

was shown to result in good statistical accuracy for all cases. For the patient case, which was both larger and more complex, a higher number of 200 million particles was chosen. All other parameters were chosen identically for the different simulations.

The beamlet-free algorithm simulates the primary protons in batches of 16 corresponding to $12.5 \cdot 10^6$ iterations of the first order algorithm for the patient case. For the comparison, a beamlet matrix with $5 \cdot 10^4$ protons per beamlet is simulated and subsequently optimized using the `scipy`¹⁹ FORTRAN implementation (wrapped in Python) of the second-order optimization algorithm L-BFGS²⁰ (Limited-memory Broyden-Fletcher-Goldfarb-Shanno algorithm). The optimizer continues until it meets the tolerance criterion which is defined as the absolute difference in objective function values between iterations and set to 10^{-4} . A final dose computation with 40 million protons is performed to match the statistical accuracy of the beamlet-free method. Both the beamlet calculation and the final dose computation are performed using the MCsquare dose engine that is also utilized in the beamlet-free algorithm. The number of primaries for the MC dose calculation in the beamlet-free algorithm was intentionally picked so that the optimized plan quality would reach the one obtained with the beamlet-based method and consequently ease the comparison.

Simulations were performed on a computation server with a total of 80 CPU cores and 526 GB RAM.

III. RESULTS

III.A. Scaling analysis

Computation time and peak memory usage are plotted against the number of spots for both methods and compared in Figure 2. The values are calculated as the mean over 5 runs and the errorbar represents the standard deviation. The difference in target coverage was less than 0.20 Gy in all cases.

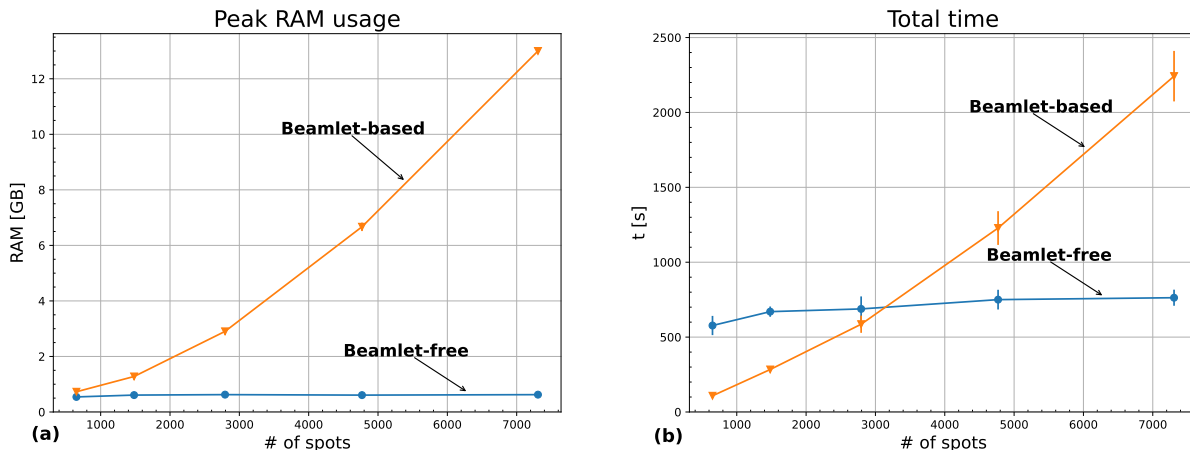


FIG. 2: Memory usage (a) and computation time (b) required by the beamlet-based and beamlet-free methods versus the number of spots for a water phantom with different target sizes.

III.B. Patient data

Dose distributions obtained by both methods are depicted in figure 3. In both cases all OAR objectives could be met and the target D_{95}/D_5 is within 5% of the prescription, as it was reported in table II.

For the OAR, D_{\max} objectives are considered as met, if the D_5 value of the ROI is below the dose limit. Similarly, D_{mean} objectives are considered as met, if the D_{mean} value of the ROI is below the dose limit. The target objectives are considered as met if the D_{95}/D_5 value is within $\pm 5\%$ of the prescription dose.

Due to the stochastic nature of both methods, small fluctuations in the final dose distributions are to be expected. The particle number and the total number of iterations have to be chosen sufficiently high to ensure an adequate level of confidence. To this end, both methods were run 5 times. The fluctuations on the target coverage, $D_5 - D_{95}$, were less than 4% for both methods.

The objective function convergence over the course of the optimization is shown in figure 4. The objective function values are plotted against the number of iteration of the respective optimization algorithm. The relative behaviour of the objective function can be compared,

Beamlet-free treatment planning

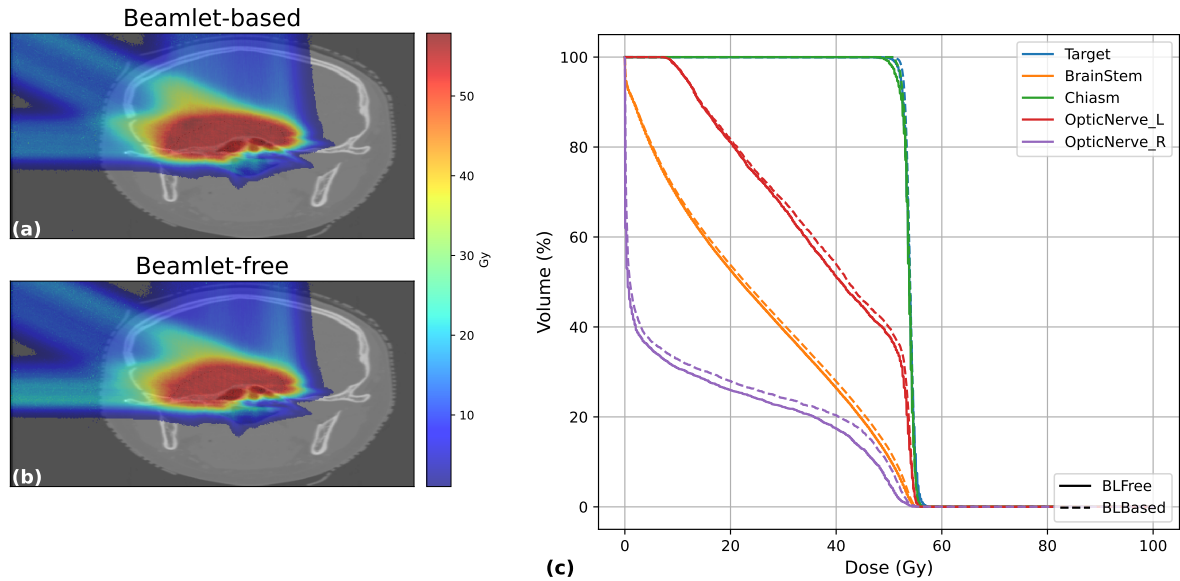


FIG. 3: Comparison of the optimized dose distribution obtained by the beamlet-based (a) and beamlet-free method (b) and the computed dose volume histogram (c) for beamlet-based (dashed) and beamlet-free (solid).

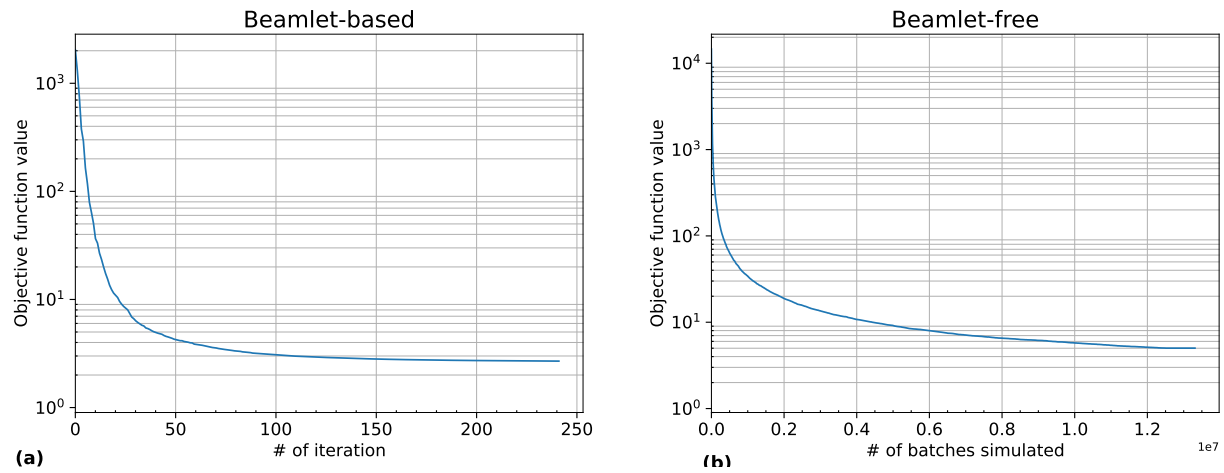


FIG. 4: (a) Convergence plot of the beamlet-based algorithm (scipy L-BFGS) and (b) convergence plot of the beamlet-free algorithm. and a similar behaviour of rapidly decreasing objective function values can be observed.

The peak memory required during the dose calculation and optimization, could be reduced from 29 GB for the beamlet-based method to about 1.561 GB for the beamlet-free method.

TABLE II: Clinical goals evaluation for the beamlet-based and beamlet-free method.

ROI	Criterion	Dose limit (Gy)	$D_{\text{Criterion}}$ (Gy) Beamlet-based	$D_{\text{Criterion}}$ (Gy) Beamlet-free
PTV	D_{95}	51.3	52.73	52.28
PTV	D_5	56.7	55.24	55.36
PTV	D_{98}	52.98	52.35	51.53
PTV	D_2	55.08	55.58	55.87
OC	D_5	60.0	55.08	55.09
OC	D_2	60.0	55.43	55.36
OC	D_{mean}	50.0	53.85	53.82
BS	D_5	55.0	53.11	52.55
BS	D_2	55.0	54.03	53.82
BS	D_{mean}	8.50	24.79	24.16
RON	D_5	55.0	51.74	49.99
RON	D_2	55.0	53.10	51.79
LON	D_5	55.0	54.57	54.58
LON	D_2	55.0	54.96	55.09

It is worth noticing that the peak memory for the beamlet-based method was recorded during the import of the individual beamlet dose distributions, compressed as sparse matrices, into the dose influence matrix (stacked as columns). Other steps in the treatment planning process, however, required higher peak memory usage than the beamlet-free method needed during dose calculation and optimization. This peak memory was recorded as about 3.569 GB. It depends on the used treatment planning system and might be improved independently from the presented algorithm. A memory comparison is drawn in Table III. Besides the peak RAM usage during simulation, it also lists the required storage disk space of the files needed for the dose calculation and optimization. The difference between the two methods with respect to utilized disk space can be explained through the storage of the large dose influence matrix that requires 4.4 GB alone.

TABLE III: Comparison of memory usage for the beamlet-based and beamlet-free method.

	Beamlet-based	Beamlet-free
Peak RAM usage [GB]	29	1.561
Storage [GB]	6.4	2.2

The total computation times averaged over 5 runs are reported in table IV.

TABLE IV: Comparison of computation time for the beamlet-based and beamlet-free method averaged over 5 runs.

	Process	t [s]
BL-based	Plan Creation	299 ± 2
	Beamlet Comp.	3356 ± 24
	Optimization	12601 ± 1714
	Final Dose Comp.	301 ± 1
	Total	16558 ± 1714
BL-free	Plan Creation	299 ± 2
	Optimization	4697 ± 129
	Total	4996 ± 129

IV. DISCUSSION

A novel treatment planning method, not limited to proton therapy, has been introduced. It merges dose calculation and optimization into a single process, resulting in improved computational efficiency and accuracy. The so-called beamlet-free algorithm was able to achieve comparable plan quality to a conventional beamlet-based algorithm.

The comparability of the two methods is limited by the fact that different parameters have to be chosen for each of them. These parameters have to be chosen in a way that allows a balance between keeping computation time low enough to enable clinical workflows while achieving a high statistical confidence. The statistical uncertainty inevitably present in MC-based treatment planning stems from the fact that MC methods, and in the case of the beamlet-free algorithm also the optimization, are based on stochastic processes. The two methods have different parameters that may be tuned to this end. For this comparison, the same number of primary protons was therefore used in the final dose calculation to ensure a comparable level of uncertainty for the MC simulation. The iteration number of the optimization algorithms is not comparable, since the direction of search is only partially estimated at each step of the beamlet-free algorithm which consequently needs a lot more iterations to converge. In both cases, the number of iterations utilized was considered as realistic to produce adequate plan quality in a reasonable time-frame. Another parameter that impacts computation time and quality of the results is the number of protons per beamlet in the beamlet-based method and the batch size in the beamlet-free. While they are hardly equivalent to one another, they play a similar role during the optimization. They

Beamlet-free treatment planning

are used as input for the optimization algorithm. Both need to be sufficiently high to prevent optimization based on inaccurate dose estimations, but still considerate of the total computation time. In beamlet-free treatment planning the three following parameters, total number of primary protons, number of iterations and batch size, depend on each other. However, they can be chosen independently in the beamlet-based case. This places some restrictions on the user, but might also be beneficial, since it reduces the risk of errors.

Both methods are able to fulfill all clinical objectives. Target coverage worsened slightly for the beamlet-free case, while OAR sparing improved for most organs. Altogether, the difference between the two methods is small, but statistically significant. It might stem from a number of sources. For example, a possible explanation could be misguided optimization steps based on insufficiently approximated gradients.

Regarding computational performances, the peak memory required during treatment planning could be reduced by 95% through the use of the beamlet-free algorithm. The total computation time could be reduced by 70% through use of the beamlet-free algorithm. Notice that the two methods profit unequally from the number of available computation threads. The MC code, MCsquare, utilizes CPU parallelization to improve computation time and is slowed down considerably, if the number of CPU threads is reduced. The beamlet-free algorithm also utilizes MCsquare for the dose simulation, but the optimization slows down the MC simulation itself. The beamlet-free algorithm still profits from having multiple CPU threads at its disposal, but especially very high numbers of threads cannot achieve comparable simulation times to the pure MC simulation. The update procedure of the mean target dose is here a bottleneck in the parallelization, that prevents the beamlet-free algorithm to draw the full benefit from very large numbers of CPU threads, probably due to conflicting accesses to the same chunks of memory. It should be noted that the presented data was obtained from simulations performed on a computation server with 80 CPU cores and that the benefit of the beamlet-free algorithm is considerably higher, for computations performed with a limited number of CPUs. For a more thorough comparison, both optimizers should be implemented within the same framework, to ensure identical conditions. Small differences can be expected by using an existing external code for the beamlet-based part (i.e. Scipy optimizer in our case) of the comparison.

The complexity analysis revealed that, in beamlet-based treatment planning, computation

Beamlet-free treatment planning

time and peak memory usage increase almost linearly with the number of spots. On the other hand, the beamlet-free method can achieve comparable plan quality without being affected by the number of spots, resulting in independent computation time and memory usage. The peak memory usage from the beamlet-free method was recorded below that of the beamlet-based simulation in all cases. With respect to computation time, for low numbers of spots the beamlet-based method outperformed the beamlet-free method, but for increasing numbers of spots, the beamlet-based method gets slowed down considerably. It is possible to determine roughly from which number of spots it would be beneficial to utilize the beamlet-free instead of a beamlet-based method. It should be kept in mind, however, that factors like the machine computations are performed on, the exact beamlet-based optimizer and implementation chosen for the comparison and the depth location of the target and number of simulated particles, can impact the two methods differently and render it impossible to fix any specific number.

It can be observed that for very low numbers of spots, the beamlet-free method can even bring disadvantages, but already for numbers of spots regularly encountered in clinical routines, the beamlet-free method starts to outperform conventional beamlet-based treatment planning. The benefits of the beamlet-free method are particularly highlighted in methods that require a large number of beamlets, such as robust optimization. In the robustness approach, traditional strategies make use of a set of worst-case scenarios^{21,22}, compiling the treatments uncertainties. If a beamlet-based approach is used, the very costly influence dose matrix must be calculated for each scenario and this further brings a computational burden during the optimization. Additionally, a more recent development sees the emergence of arc proton therapy treatment modality²³⁻²⁶ that delivers the dose across a very large set of irradiation angles, shaping the arc. However, increasing the number of beams translates into increasing the number of spots, resulting in producing a larger beamlet matrix than the “classical” one obtained with an IMPT treatment. Finally, the beamlet-free method could also play an interesting role for adaptive proton therapy where a new treatment plan might be needed in good time for an anatomy that has changed.

V. CONCLUSION

The proposed beamlet-free algorithm could successfully generate treatment plans of comparable quality to conventional treatment planning methods. Memory requirements could be reduced by 95% and the computation time by 70% on an illustrative patient case. The scaling analysis revealed that the benefit to be drawn from the beamlet-free method increases for higher numbers of spots, which makes the method promising for new emerging treatment techniques such as robust optimization, adaptive and arc proton therapy.

VI. ACKNOWLEDGMENTS

D.P. is funded through a Télévie grant by the F.R.S.-FNRS (Fonds de la Recherche scientifique). S.W. is funded by the Walloon Region as part of the Arc Proton Therapy convention (Pôles Mecatech et Biowin). J.A.L. is a Research Director with the F.R.S.-FNRS (Fonds de la Recherche scientifique).

VII. CONFLICT OF INTEREST

Kevin Souris is an employee at Ion Beam Applications SA.

REFERENCES

- ¹H. M. Kooy and C. Grassberger, Intensity modulated proton therapy, *The British Journal of Radiology* **88**, 20150195 (2015), PMID: 26084352.
- ²L. Hong, M. Goitein, M. Bucciolini, R. Comiskey, B. Gottschalk, S. Rosenthal, C. Serago, and M. Urie, A pencil beam algorithm for proton dose calculations, *Physics in Medicine & Biology* **41**, 1305 (1996).
- ³H. Paganetti, Range uncertainties in proton therapy and the role of Monte Carlo simulations, *Physics in Medicine & Biology* **57**, R99 (2012).
- ⁴K. S. F. . F. D. S. Taylor, P. A., Pencil Beam Algorithms Are Unsuitable for Proton Dose Calculations in Lung, *International journal of radiation oncology, biology, physics* **99**, 750–756 (2017).

- ⁵M. Fippel and M. Soukup, A Monte Carlo dose calculation algorithm for proton therapy, *Medical Physics* **31**, 2263–2273 (2004).
- ⁶A. Tourovsky, A. J. Lomax, U. Schneider, and E. Pedroni, Monte Carlo dose calculations for spot scanned proton therapy, *Physics in Medicine & Biology* **50**, 971 (2005).
- ⁷R. Kohno, K. Hotta, S. Nishioka, K. Matsubara, R. Tansho, and T. Suzuki, Clinical implementation of a GPU-based simplified Monte Carlo method for a treatment planning system of proton beam therapy, *Physics in Medicine & Biology* **56**, N287 (2011).
- ⁸K. Jabbari and J. Seuntjens, A fast Monte Carlo code for proton transport in radiation therapy based on MCNPX, *Journal of Medical Physics* **39**, 156–163 (2014).
- ⁹K. Souris, J. A. Lee, and E. Sterpin, Fast multipurpose Monte Carlo simulation for proton therapy using multi- and many-core CPU architectures, *Medical Physics* **43**, 1700–1712 (2016).
- ¹⁰A. Schiavi, M. Senzacqua, S. Pioli, A. Mairani, G. Magro, S. Molinelli, M. Ciocca, G. Battistoni, and V. Patera, Fred: a GPU-accelerated fast-Monte Carlo code for rapid treatment plan recalculation in ion beam therapy, *Physics in Medicine & Biology* **62**, 7482 (2017).
- ¹¹P. Ziegenhein, J. J. Wilkens, S. Nill, T. Ludwig, and U. Oelfke, Speed optimized influence matrix processing in inverse treatment planning tools, *Physics in Medicine & Biology* **53**, N157 (2008).
- ¹²U. Oelfke and T. Bortfeld, Inverse planning for photon and proton beams, *Medical Dosimetry* **26**, 113–124 (2001).
- ¹³H. E. Robbins, A Stochastic Approximation Method, *Annals of Mathematical Statistics* **22**, 400–407 (1951).
- ¹⁴S. Wuyckens, D. Dasnoy, G. Janssens, V. Hamaide, M. Huet, E. Loÿen, G. R. de Hertaing, B. Macq, E. Sterpin, J. A. Lee, K. Souris, and S. Deffet, OpenTPS – Open-source treatment planning system for research in proton therapy, 2023.
- ¹⁵C. G. BROYDEN, The Convergence of a Class of Double-rank Minimization Algorithms 1. General Considerations, *IMA Journal of Applied Mathematics* **6**, 76–90 (1970).
- ¹⁶D. Shanno, Conditioning of quasi-Newton methods for function minimization, *Mathematics of Computation*. **24**, 647–656 (1970).
- ¹⁷D. Goldfarb, A family of variable-metric methods derived by variational means, *Mathematics of Computation*. **24**, 23–26 (1970).

- ¹⁸R. Fletcher, A new approach to variable metric algorithms, *The Computer Journal* **13**, 317–322 (1970).
- ¹⁹P. Virtanen et al., SciPy 1.0: Fundamental Algorithms for Scientific Computing in Python, *Nature Methods* **17**, 261–272 (2020).
- ²⁰D. Liu and J. Nocedal, On the limited memory BFGS method for large scale optimization, *Mathematical Programming* **45**, 503–528 (1989).
- ²¹J. Unkelbach, T. C. Y. Chan, and T. Bortfeld, Accounting for range uncertainties in the optimization of intensity modulated proton therapy, *Physics in Medicine & Biology* **52**, 2755 (2007).
- ²²D. Pflugfelder, J. J. Wilkens, and U. Oelfke, Worst case optimization: a method to account for uncertainties in the optimization of intensity modulated proton therapy, *Physics in Medicine & Biology* **53**, 1689 (2008).
- ²³X. Ding, X. Li, J. M. Zhang, P. Kabolizadeh, C. Stevens, and D. Yan, Spot-Scanning Proton Arc (SPArc) Therapy: The First Robust and Delivery-Efficient Spot-Scanning Proton Arc Therapy, *International Journal of Radiation Oncology*Biography*Physics* **96**, 1107–1116 (2016).
- ²⁴W. Gu, D. Ruan, Q. Lyu, W. Zou, L. Dong, and K. Sheng, A novel energy layer optimization framework for spot-scanning proton arc therapy, *Medical physics* **47**, 2072–2084 (2020).
- ²⁵E. Engwall, C. Battinelli, V. Wase, O. Marthin, L. Glimelius, R. Bokrantz, B. Andersson, and A. Fredriksson, Fast robust optimization of proton PBS arc therapy plans using early energy layer selection and spot assignment, *Physics in Medicine & Biology* **67**, 065010 (2022).
- ²⁶S. Wuyckens, M. Saint-Guillain, G. Janssens, L. Zhao, X. Li, X. Ding, E. Sterpin, J. A. Lee, and K. Souris, Treatment planning in arc proton therapy: Comparison of several optimization problem statements and their corresponding solvers, *Computers in Biology and Medicine* , 105609 (2022).